© 2020. Published by The Company of Biologists Ltd | Development (2020) 147, dev194316. doi:10.1242/dev.194316

RESEARCH REPORT

Increased lateral tension is sufficient for epithelial folding in *Drosophila*

Liyuan Sui[1] and Christian Dahmann[1,2,*]

ABSTRACT

The folding of epithelial sheets is important for tissues, organs and embryos to attain their proper shapes. Epithelial folding requires subcellular modulations of mechanical forces in cells. Fold formation has mainly been attributed to mechanical force generation at apical cell sides, but several studies indicate a role of mechanical tension at lateral cell sides in this process. However, whether lateral tension increase is sufficient to drive epithelial folding remains unclear. Here, we have used optogenetics to locally increase mechanical force generation at apical, lateral or basal sides of epithelial *Drosophila* wing disc cells, an important model for studying morphogenesis. We show that optogenetic recruitment of RhoGEF2 to apical, lateral or basal cell sides leads to local accumulation of F-actin and increase in mechanical tension. Increased lateral tension, but not increased apical or basal tension, results in sizeable fold formation. Our results stress the diversification of folding mechanisms between different tissues and highlight the importance of lateral tension increase for epithelial folding.

KEY WORDS: Epithelial folding, Mechanical tension, Optogenetics, RhoGEF2, Wing disc, *Drosophila*

INTRODUCTION

The sculpting of tissues is important for animal morphogenesis (Gilmour et al., 2017). Shape changes of developing animals are often driven by the coordinated reshaping of epithelial cells that cover the surface and inner organs of the animal. A fundamental shape change of epithelia is folding, which deforms the quasi two-dimensional cell sheet into a three-dimensional structure (Anlas and Nelson, 2018; Martin and Goldstein, 2014; Pearl et al., 2017; Sawyer et al., 2010; Zartman and Shvartsman, 2010). Epithelial folding is important in embryos, e.g. during gastrulation (Gilmour et al., 2017) and neural tube (Nikolopoulou et al., 2017), eye (Chauhan et al., 2015), gut (Shyer et al., 2013) and brain (Long et al., 2018) development. Defects in neural tube formation are associated with severe human disorders (Wallingford et al., 2013).

One mechanism by which epithelial sheets fold is the coordinated constriction of the apical sides of cells (Martin and Goldstein, 2014; Pearl et al., 2017; Sawyer et al., 2010). Apical cell constriction depends on the contraction of a filamentous (F-)actin meshwork through the activity of non-muscle myosin II (Myosin II). Activation of Myosin II commonly depends on the small GTPase Rho and its guanine-nucleotide-exchange factors (RhoGEFs) (Agarwal and Zaidel-Bar, 2019). This contractile actomyosin meshwork localizes to the medioapical side of cells and is connected to the adherens junctions (Heer and Martin, 2017; Martin et al., 2009). Apical cell constriction results in a wedge-like cell shape that, when coordinated among neighboring cells, can result in fold formation.

A further mechanism involved in epithelial folding is lateral constriction of cells (Pearl et al., 2017). Accumulations of actomyosin at lateral cell interfaces generate contractile forces along the lateral side of cells, leading to cell height decrease. Lateral constriction has, for example, been observed during ascidian gastrulation (Sherrard et al., 2010), during folding of the *Drosophila* embryonic epidermis at parasegment boundaries (Urbano et al., 2018) and within the cephalic furrow (Eritano et al., 2020; Spencer et al., 2015), during epithelial folding of the *Drosophila* wing disc (Sui et al., 2018) and leg disc (Ambrosini et al., 2019; Monier et al., 2015), and in conjunction with apical cell constriction during ventral furrow formation of the *Drosophila* embryo (Gracia et al., 2019). Ablation of lateral cell interfaces impairs furrow formation (Gracia et al., 2019), showing that lateral constriction is required for ventral furrowing. It is not known whether lateral constriction by itself is sufficient to drive epithelial folding.

The larval *Drosophila* wing disc is a useful model system for studying epithelial folding. The larval wing disc is a single cell-layered epithelium that gives rise to parts of the body wall and the wing blade (Cohen, 1993). During mid-larval development, one major fold forms between the prospective body wall and wing blade regions of the wing disc (known as the hinge/pouch or H/P fold). In a previous study, we showed that formation of this fold does not involve apical cell constriction (Sui et al., 2018), raising the question as to whether apical cell constriction, in principle, could suffice for fold formation in this tissue. Indeed, simulations of force balances using a three-dimensional vertex model accounting for the geometry of wing disc cells indicate that increased mechanical tension at the apical sides of cells is inefficient in driving folding (Sui et al., 2018). Instead, the formation of this H/P fold is characterized by lateral cell constriction resulting in decreased cell height (i.e. apicobasal cell length) and basal cell widening. Lateral cell constriction is associated with flows of F-actin along the lateral surfaces of cells and increased lateral surface tension (Sui et al., 2018). It is unknown whether a local increase in lateral tension is sufficient to drive fold formation in wing discs.

Here, we have used optogenetics to systematically test whether force generation at apical, basal or lateral sides of *Drosophila* wing disc cells is sufficient for fold formation. We show that spatially confined photoactivation of RhoGEF2 results in the specific increase of apical, basal or lateral tension. We find that increased lateral force generation is sufficient to form deep folds, whereas increased apical or basal force generation results in only minor folding.

[1]Institute of Genetics, Technische Universität Dresden, 01062 Dresden, Germany. [2]Cluster of Excellence Physics of Life, Technische Universität Dresden, 01062 Dresden, Germany.

*Author for correspondence (christian.dahmann@tu-dresden.de)

C.D., 0000-0001-6822-0964

Handling Editor: Thomas Lecuit
Received 19 June 2020; Accepted 16 October 2020

Development (2020) 147, dev194316. doi:10.1242/dev.194316

RESULTS AND DISCUSSION

RhoGEF2 photoactivation results in a spatially controlled accumulation of F-actin

To test whether a local increase in apical, basal or lateral tension is sufficient to drive fold formation in wing discs, we sought to spatially control force generation by employing optogenetic activation of RhoGEF2. RhoGEF2 stimulates both F-actin polymerization and Myosin II motor activity to increase actomyosin contractility (Agarwal and Zaidel-Bar, 2019). Recent work has established and implemented an optogenetic method to increase actomyosin contractility with high spatiotemporal control in *Drosophila* embryos (Izquierdo et al., 2018). This method is based on the blue light-dependent binding of Cryptochrome 2 (CRY2) to the N-terminal region of the CIB protein (CIBN) that is targeted to the plasma membrane (pm) via a CaaX anchor. Blue light illumination recruits the cytosolic CRY2 to the plasma membrane (Fig. 1A). We expressed a RhoGEF2-CRY2 fusion protein and a CIBN::pmGFP fusion protein under control of the Gal4-UAS system (Brand and Perrimon, 1993) in wing discs. *Ex vivo* cultured wing discs were illuminated using a two-photon excitation laser scanning microscope for 2 min with light of wavelength λ=950 nm (henceforth referred to as 'blue light') at the apical, lateral or basal regions of cells co-expressing RhoGEF2-CRY2 and CIBN::pmGFP (see Materials and Methods; Fig. 1B). Illumination was confined to the pouch region of the wing disc, which normally does not undergo folding.

We first tested whether blue light illumination resulted in a spatially controllable accumulation of F-actin in wing disc cells. F-actin was visualized using the F-actin binding domain of Moesin fused to mCherry (MoeABD::mCherry). Apical illumination resulted in the apical accumulation of F-actin, whereas lateral and basal illumination resulted in the lateral and basal accumulation of F-actin, respectively (Fig. 1C-E‴; Movie 1). F-actin accumulation was confined to the illuminated region (Fig. 1C-E‴). In each case, accumulation of F-actin was most pronounced directly after illumination, and declined within ∼10 min to the level observed prior to illumination (Fig. 1F-K). These results show that photoactivation of RhoGEF2 results in a reversible, spatially controllable accumulation of F-actin in wing discs.

RhoGEF2 photoactivation results in a spatially controlled increase of mechanical tension

We next tested whether blue light illumination resulted in a spatially controllable increase of mechanical tension. We first measured mechanical tension at adherens junctions (henceforth referred to as apical cell edges) and at basal cell edges by laser ablation of single cell edges. Severing an apical or a basal cell edge results in tissue relaxation and the displacement of the two ends (vertices) of the ablated cell edge in the plane of the tissue (Farhadifar et al., 2007; Ma et al., 2009; Sui et al., 2018). We measured the vertex distance increase over time and the initial recoil velocity of displacement. The initial recoil velocity of displacement is a relative measure of the mechanical tension that was exerted on the cell edge before it was cut. *Ex vivo* cultured wing discs co-expressing RhoGEF2-CRY2 and CIBN::pmGFP were oriented with their apical or basal side facing towards the microscope objective and illuminated with blue light at the apical or basal region, respectively, for 2 min. Cell edges were immediately ablated thereafter. Cell membranes were marked by Gap43::mCherry. Wing discs of the same genotype that were not illuminated with blue light served as negative controls. In control wing discs, ablation of basal cell edges resulted in a greater final vertex displacement and faster recoil velocity when compared with the ablation of apical cell edges (Fig. 2A,A′,C,C′,I,J,L,M), consistent with a previous report (Sui et al., 2018). Blue light activation to recruit RhoGEF2 to apical or basal cell edges resulted in an increased final vertex displacement and faster initial recoil velocity compared with those of controls (Fig. 2B,B′,D,D′,I,J,L,M; Movie 2). Recoil velocity upon ablation of apical cell edges was increased ∼threefold (Fig. 2I), whereas recoil velocity upon ablation of basal cell edges was increased ∼1.5-fold (Fig. 2J). These data show that optogenetic recruitment of RhoGEF2 to apical and basal cell edges results in approximately threefold increased apical cell edge tension and 1.5-fold increased basal cell edge tension.

We next measured lateral surface tension. F-actin was visualized using MoeABD::mCherry. *Ex vivo* cultured wing discs were oriented with the lateral side towards the microscope objective, and lateral cell interfaces were illuminated with blue light for 2 min and then immediately ablated. Severing a lateral cell edge results in tissue relaxation and the displacement of the vertices of the ablated cell edge along the apicobasal axis of the tissue, leading to an increase in the distance between the apical and basal cell surfaces at the site of ablation. We measured the increase in distance between the apical and basal vertices of the cell edge upon ablation and the initial velocity of this recoil. In controls, where wing discs were not illuminated with blue light, ablation of lateral cell interfaces resulted in a barely detectable recoil (Fig. 2E,E′,G,K,N), as shown previously (Sui et al., 2018). By contrast, after blue light illumination to recruit RhoGEF2 to lateral cell sides, the recoil upon laser ablation was greatly increased (Fig. 2F,F′,H,K,N; Movie 3). Recoil velocity was increased approximately tenfold upon blue light illumination (Fig. 2K). These data show that optogenetic recruitment of RhoGEF2 to lateral cell sides results in increased lateral surface tension. Taken together, we conclude that RhoGEF2 photoactivation allows a spatially controllable increase in mechanical tension.

Lateral RhoGEF2 photoactivation is sufficient for fold formation

To test whether apical or basal photoactivation of RhoGEF2 results in apical or basal constriction of wing disc cells, we analyzed the apical and basal cross-sectional area of cells upon blue light illumination. *Ex vivo* cultured wing discs co-expressing RhoGEF2-CRY2 and CIBN::pmGFP were illuminated with blue light at the apical or basal region, and the apical and basal cross-sectional areas of illuminated cells were analyzed. Cell membranes were visualized using CIBN::pmGFP. Apical blue light illumination led to ∼60% decrease of apical cross-sectional area of cells within 100 s (Fig. 3A, C; Movie 4). Basal blue light illumination resulted in ∼30% decrease of basal cross-sectional area (Fig. 3B,D; Movie 4). Thus, apical and basal photoactivation of RhoGEF2 drives apical and basal cell constriction, respectively.

We next tested whether apical, basal or lateral photoactivation of RhoGEF2 results in epithelial fold formation. Folds are characterized by the apical or basal indentation of the epithelium and often a reduced height of cells inside the fold as compared with those outside the fold. We therefore measured cell height and apical and basal indentation of the tissue upon blue light illumination (Fig. 3E). Cell shapes were visualized using Gap43::mCherry. Apical illumination resulted in a shallow apical indentation of the tissue (Fig. 3F-F‴,I; Fig. S1A-A‴). A basal indentation was not detectable (Fig. 3F,I). Cell height was reduced by ∼8% (Fig. 3I). Basal illumination resulted in a shallow basal indentation, as well as a weak apical indentation (Figs. 3G-G‴,J; Fig. S1B-B‴). Cell height was reduced by ∼21% (Fig. 3J). Finally, lateral illumination resulted in a strong apical

Development (2020) 147, dev194316. doi:10.1242/dev.194316

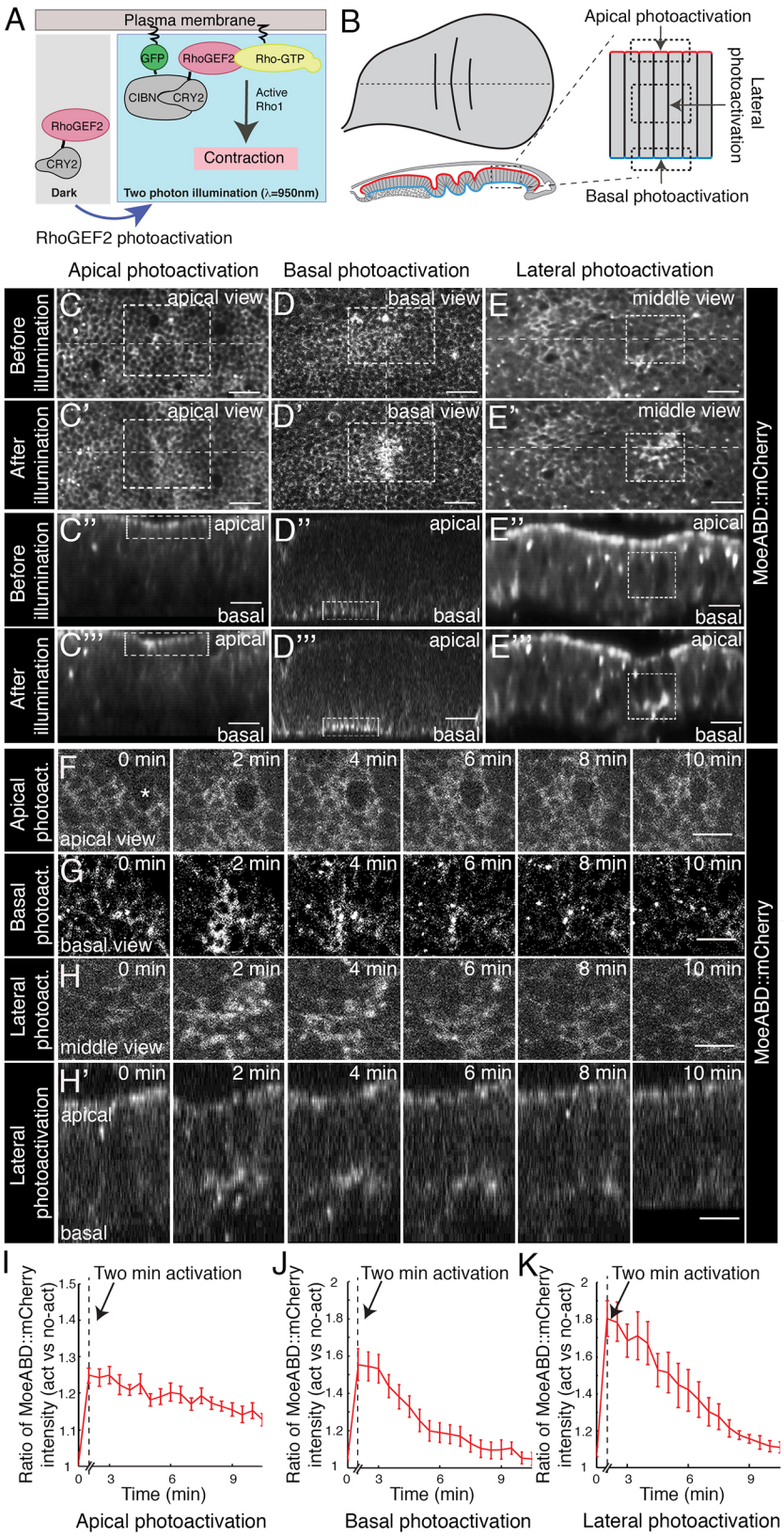

Fig. 1. RhoGEF2 photoactivation results in a spatially controlled accumulation of F-actin. (A) Schematic illustrating blue light-dependent recruitment of RhoGEF2 to the plasma membrane. (B) Schematics illustrating the regions of the wing disc that were illuminated by blue light. (C-E‴) Top views (C,C′,D,D′,E,E′) and cross-sectional views (C″,C‴,D″, D‴,E″,E‴) of wing discs expressing RhoGEF2-CRY2 and CIBN::pmGFP before and after a 2 min illumination with blue light in the indicated region (dashed boxes). MoeABD::mCherry, a marker for F-actin, is shown. C,C′ show apical views; D,D′ show a basal view; E,E′ show a view 15 µm beneath the apical surface (middle view). Dashed lines indicate corresponding positions of cross-sectional views. Scale bars: 10 µm. (F-H′) Top views (F-H) and cross-sectional view (H′) of wing discs with the genotype as in C-E‴, before and at the indicated times after the onset of a 2 min illumination with blue light. F shows an apical view; G shows a basal view; H shows a view 15 µm beneath the apical surface (middle view). MoeABD::mCherry is shown. The cell with the large apical area (asterisk in F) is a diving cell. Scale bars: 10 µm. (I-K) MoeABD::mCherry pixel intensity before and at the indicated times after the onset of a 2 min illumination by blue light. The intensities for each time point are presented as the ratio of intensities in the activated region and an adjacent non-activated region (act versus no-act). Mean±s.e.m., n=9 regions in three wing discs each for I-K. Dashed line indicates the end of photoactivation.

indentation and a weaker basal indentation (Figs. 3H-H‴,K; Fig. S1C-C‴). Cell height was reduced by ∼35% (Fig. 3K). We conclude that photoactivation of RhoGEF2 at lateral cell sides is sufficient to form deep folds. Apical or basal photoactivation, under our experimental conditions, results only in shallow folds.

Repeated lateral RhoGEF2 photoactivation results in a long-lasting and reversible fold formation

We next tested how long the cell shape changes induced by lateral photoactivation lasted. *Ex vivo* cultured wing discs co-expressing RhoGEF2-CRY2 and CIBN::pmGFP were illuminated with blue

Development (2020) 147, dev194316. doi:10.1242/dev.194316

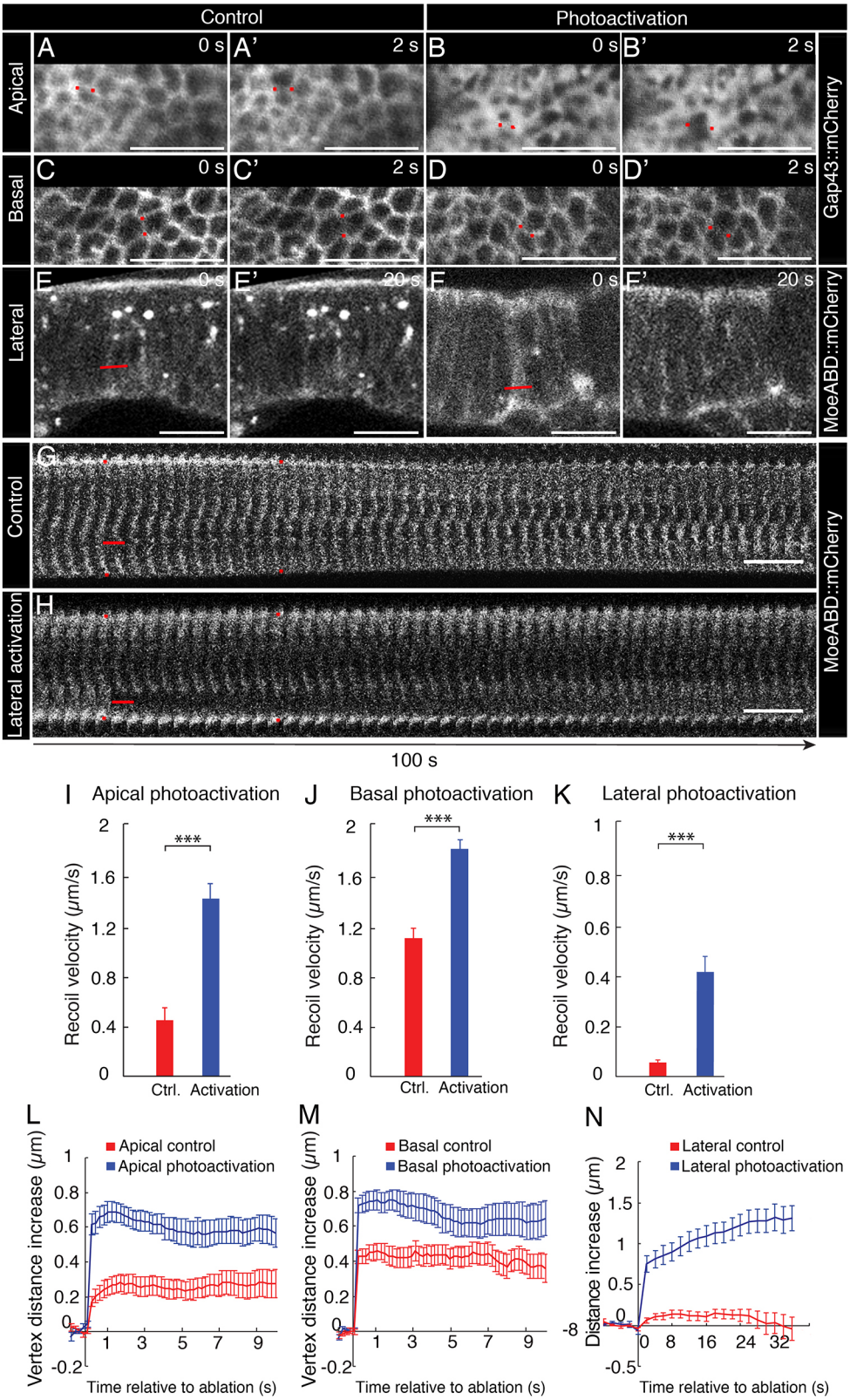

Fig. 2. RhoGEF2 photoactivation results in a spatially controlled increase of mechanical tension. (A-F′) Top views (A-D′) and cross-sectional views (E-F′) of wing discs expressing RhoGEF2-CRY2 and CIBN::pmGFP before and at the indicated time after laser ablation. Photoactivation samples were treated with 2 min blue light illumination immediately before laser ablation. Control samples received no blue light illumination. Cell edges are visualized using Gap43::mCherry (A-D′) or MoeABD::mCherry (E-F′). Red dots indicate the two vertices of the ablated cell edge; red lines indicate positions of laser cuts. Scale bars: 10 µm. (G,H) Kymograms of lateral laser ablations as detailed in E-F′. Red dots indicate the apical and basal vertices of the ablated cell edge immediately before and 20 s after ablation. Red lines indicate position of laser cuts. (I-K) Average recoil velocity of the two vertices at the end of an ablated cell edge for wing discs of the genotype and conditions detailed in A-F′. Recoil velocity was measured in the plane (I,J) or along the apical-basal axis (K) of the tissue. Data are mean±s.e.m., n=15 cuts for each location and condition, except for the control (Ctrl) in K, where n=10 cuts. ***P<0.001 (Mann–Whitney U test). (L-N) Increase in the distance between two vertices at the end of an ablated cell edge as described in I-K, as a function of time relative to ablation. Data are mean±s.e.m., n=15 cuts for each location and condition, except for the control in N, where n=10 cuts.

light at the lateral region for 2 min, and cell height and MoeABD::mCherry intensity were measured over time. During the 2 min period of illumination, cell height shrank to ~86% of its initial value (Fig. 4A). At 4 min after the end of illumination, cell height was recovered to ~89% of its initial value. By ~10 min after illumination, cell height was fully recovered to its initial length (Fig. 4A). Recovery of cell height paralleled the loss of blue light-induced F-actin accumulation (Fig. 4A). We next sought to maintain fold formation for longer periods of time. To this end, we repeatedly (six times) illuminated wing discs at the lateral region with blue

Development (2020) 147, dev194316. doi:10.1242/dev.194316

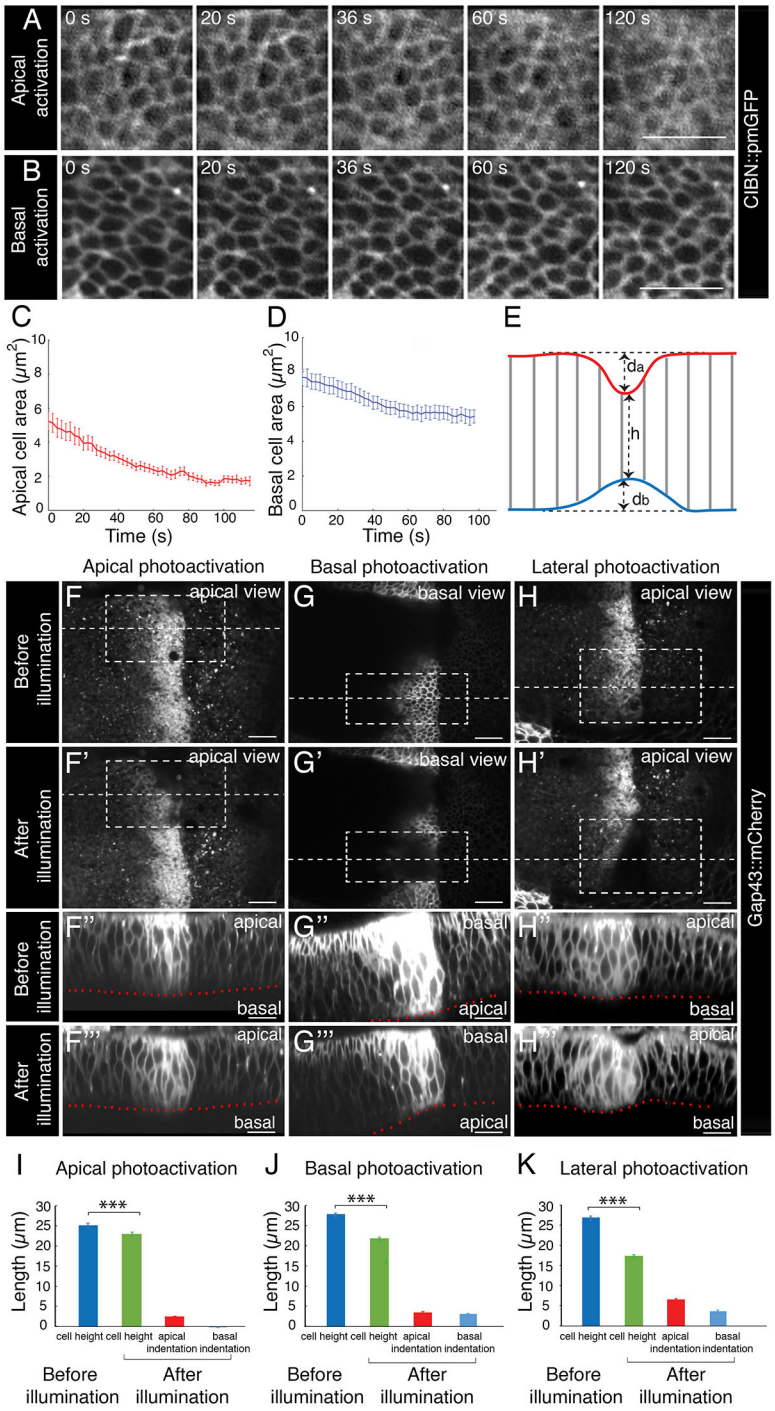

Fig. 3. Lateral RhoGEF2 photoactivation is more effective in fold formation than apical or basal photoactivation. (A,B) Apical (A) and basal (B) views of wing discs expressing RhoGEF2-CRY2 and CIBN::pmGFP before and during illumination with blue light at the apical (A) or basal (B) region of cells. Time after onset of a 2 min illumination is indicated. CIBN::pmGFP marks cell membranes. Scale bars: 10 µm. (C,D) Apical (C) and basal (D) cross-sectional area of wing disc cells expressing RhoGEF2-CRY2 and CIBN::pmGFP as a function of time after the onset of illumination with blue light at the apical (C) or basal (D) region of cells. Data are mean±s.e.m., *n*=20 cells of three wing discs for C, *n*=25 cells of three wing discs for D. (E) Schematic of a cross-sectional view of a wing disc illustrating measurements of apical indentation d_a, basal indentation d_b and cell height *h*. (F-H‴) Top views (F,F′,G,G′,H,H′) and cross-sectional views (F″,F‴,G″,G‴,H″,H‴) of wing discs expressing RhoGEF2-CRY2 and CIBN::pmGFP under control of *ptc-Gal4*, before and after a 2 min illumination with blue light in the indicated regions (dashed boxes). Dashed lines indicate corresponding positions of cross-sections shown in cross-sectional views. Red dotted lines in F″, F‴, H″ and H‴ mark basal edges of wing discs. Red dotted lines in G″ and G‴ mark apical edges of wing discs. Gap43::mCherry marks cell membranes. Scale bars: 10 µm. (I-K) Cell height (*h* in E) before illumination and cell height, apical indentation (d_a in E) and basal indentation (d_b in E) after a 2 min illumination with blue light of apical (I), basal (J) or lateral (K) regions of cells. Data are mean±s.e.m., *n*=12 cross-sections of three wing discs each for I-K. ***P<0.001 (Wilcoxon signed-rank test).

light. Each 2 min illumination was followed by a 4 min interval of no illumination (Fig. 4B). After the final period of illumination, the wing disc was observed for another 28 min. During the first period of blue light illumination, an apical and, to a lesser extent, basal indentation formed in the tissue and cell height was reduced, indicating that a fold had formed (Fig. 4C,D). During the following five repetitions of blue light illumination, cell height further decreased, indicating that the depth of the fold increased (Fig. 4C, D). During the 28 min following the last blue light illumination, the fold receded and the initial height and shape of the wing disc was recovered (Fig. 4C,D; Movie 5). We conclude that repeated photoactivation of RhoGEF2 allows for a longer lasting, but still reversible, fold formation. The reversibility of the ectopic fold indicates an elastic behavior of the wing disc at the timescale analyzed. Similarly, recent experiments on Caco-2 monolayers showed that pulsatile photoactivation of RhoA leading to low contractile stress results in reversible junctional deformation. High contractile stress, on the other hand, leads to permanent junction shortening involving the remodeling of slackened membrane by endocytosis (Cavanaugh et al., 2020; Staddon et al., 2019). It will be interesting to test whether a higher-level increase of lateral tension will result in permanent deformations of wing discs, paving the way to reconstruct epithelial morphogenesis in this model tissue (Krueger et al., 2019).

Development (2020) 147, dev194316. doi:10.1242/dev.194316

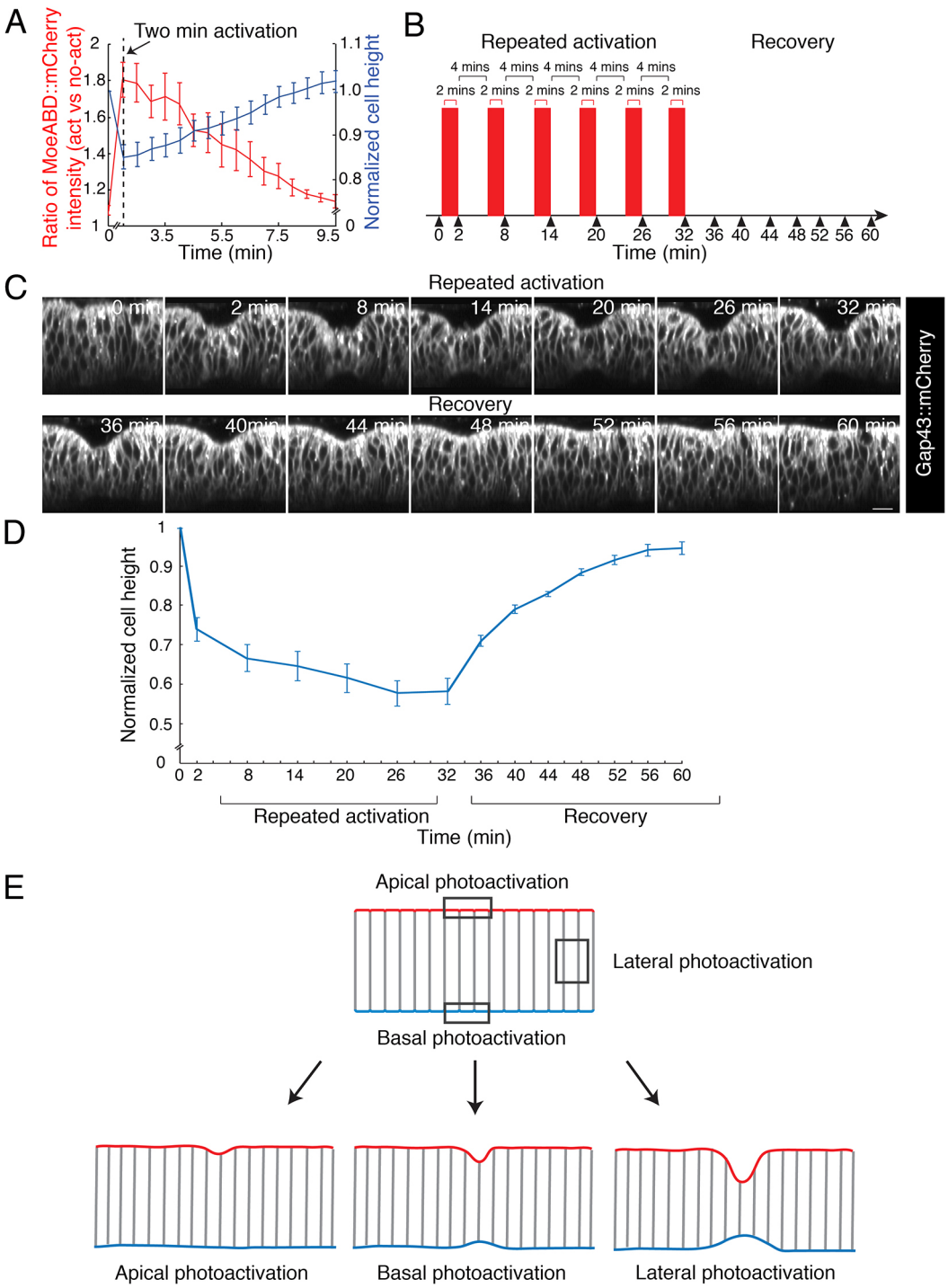

Fig. 4. Repeated lateral RhoGEF2 photoactivation results in a long-lasting and reversible fold formation. (A) Normalized MoeABD::mCherry pixel intensity (for comparison replotted from Fig. 1K) and cell height as a function of time after onset of a 2 min illumination of the lateral region of cells. Cell height is normalized to the time point before illumination. Data are mean±s.e.m., *n*=9 regions in three wing discs. (B) Schematic illustrating the approach of repeated photoactivation and recovery. Red bars indicate time periods of illumination. (C) Images of a time-lapse movie. Cross-sectional views of wing discs expressing RhoGEF2-CRY2 and CIBN::pmGFP are shown. Apical is to the top. Times of illumination of the lateral region are as indicated in B. Gap43::mCherry marks cell membranes. Scale bar: 10 µm. (D) Normalized cell height as a function of time for wing discs undergoing repeated photoactivation and recovery as indicated in B. Values are normalized as in A. Data are mean±s.e.m., *n*=9 cross-sections of three wing discs. (E) Diagrams showing that lateral RhoGEF2 photoactivation is more effective than apical or basal photoactivation in driving fold formation in wing discs.

We provide evidence that an increased lateral tension on its own can drive deep epithelial invagination and folding of *Drosophila* wing discs (Fig. 4E). These findings are consistent with simulations of force balances using vertex models (Sui et al., 2018; Wen et al., 2017). We also show that apical photoactivation of RhoGEF2 results in apical F-actin accumulation, increased apical tension and apical cell constriction, but only in a shallow fold formation. These results indicate that apical cell constriction is inefficient for fold

Development (2020) 147, dev194316. doi:10.1242/dev.194316

formation in wing discs. This notion is consistent with our previous findings that fold formation in the prospective hinge region of the wing discs does not involve apical cell constriction (Sui et al., 2018). In contrast, fold formation in the embryonic *Drosophila* epidermis (ventral furrow) does involve apical cell constriction, and photoactivation of RhoGEF2 at apical sides is sufficient to form a deep invagination (Izquierdo et al., 2018). Taken together, these data indicate that different epithelia require, and may thus employ, different mechanisms to efficiently form a fold. Future work will be required to reveal the cellular and tissue properties that, in a given tissue, make one mechanism more efficient than others in driving epithelial folding.

MATERIALS AND METHODS

Fly stocks and genetics

The following fly stocks were used: *UASp-CIBN::pmGFP* (a gift from Stefano De Renzis, EMBL, Heidelberg, Germany) (Guglielmi et al., 2015), *UASp-RhoGEF2-CRY2* (a gift from Stefano De Renzis) (Izquierdo et al., 2018), *UAS-sqh-Gap43::mCherry* (Booth et al., 2014), *ptc-Gal4* (a gift from Elisabeth Knust, Max Planck Institute of Molecular Cell Biology and Genetics, Dresden, Germany), *ap-Gal4* (a gift from Elisabeth Knust), *tub-Gal80^{ts}* (McGuire et al., 2003) and *sqh-MoeABD::mCherry* (Bloomington *Drosophila* Stock Center line 35521). All fly stocks and crosses were kept at 22°C unless indicated otherwise. All crosses were maintained in the dark.

The genotypes of larvae were as follows. To visualize F-actin upon RhoGEF2 activation (Fig. 1C-H′): *ptc-Gal4, UASp-CIBN::pmGFP; UASp-RhoGEF2-CRY2/sqh-MoeABD::mCherry*. To ablate apical and basal cell edges upon RhoGEF2 activation (Fig. 2A-D′): *ap-Gal4, tub-Gal80^{ts}, UASp-CIBN::pmGFP; UASp-RhoGEF2-CRY2/sqh-Gap43::mCherry*. Larvae were incubated at 22°C and transferred to 29°C for 3 days before dissection. To ablate lateral F-actin cables upon RhoGEF2 activation (Fig. 2E-H): *ptc-Gal4, UASp-CIBN::pmGFP; UASp-RhoGEF2-CRY2/sqh-MoeABD::mCherry*. To visualize cell shape upon RhoGEF2 activation (Fig. 3A,B,F-H′): *ptc-Gal4, UASp-CIBN::pmGFP; UASp-RhoGEF2-CRY2/sqh-Gap43::mCherry*. To visualize cell shape upon repeated RhoGEF2 activation (Fig. 4C,D): *ap-Gal4, tub-Gal80^{ts}, UASp-CIBN::pmGFP; UASp-RhoGEF2-CRY2/sqh-Gap43::mCherry*. Larvae were incubated at 22°C and transferred to 29°C for 3 days before dissection.

Live imaging of wing discs and optogenetics

All larvae were kept in the dark. Early third instar larvae were identified and dissected using a standard dissection microscope under transmitted illumination. A red filter was set up in front of the microscope light source to prevent unwanted photoactivation. Wing discs were dissected and cultured in cultured medium as described previously (Sui et al., 2018). Wing discs were placed in glass-bottomed Petri dishes (Matek). Imaging and two-photon activation experiments were performed using a multiphoton laser scanning microscope Zeiss LSM 710 NLO, using a C-Apochromat 40×/1.2 W objective. The pouch region of wing discs was analyzed.

MoeABD::mCherry and Gap43::mCherry were used for visualization of F-actin and cell membranes, respectively. For all experiments, an initial *z*-stack in the mCherry channel (acquisition at 561 nm) was acquired (60 planes, 1 µm spacing) prior to activation. Local two-photon photoactivation was achieved at 950 nm with laser power set to 13 mW and scanning direction set to bidirectional, yielding a pixel dwell of 3.15 µs. For apical or basal activation, wing discs were mounted with their apical or basal side facing to the objective, respectively. A region of interest (ROI) was defined in the pouch region of wing discs, the cell apical or basal surface was photoactivated within five image slices, each 1 µm apart, for 50 frames (total activation time of around 120 s) per activation cycle. For lateral activation, wing discs were mounted with their apical side facing to the objective. A ROI was defined in the pouch region of the wing disc, and a middle focal volume encompassing ten slices, each 1 µm apart, for 25 frames (total activation time of around 120 s) per activation cycle was photoactivated (apical and basal surfaces of cells were excluded). After photoactivation, an entire *z*-stack was acquired (60 planes, 1 µm spacing) in the mCherry channel (acquisition at 561 nm) again. For repeated lateral activation experiments, six activation cycles were used with 4 min interval times at the end of each activation cycle.

Laser ablation

Apical and basal

For apical and basal laser ablation experiments, wing discs were mounted in culture medium as described previously (Sui et al., 2018). Cell edges were visualized using Gap43::mCherry. For cutting apical cell edges, the apical side was facing the objective. For cutting basal cell edges, the basal side was facing the objective. Before laser ablation, one cycle of photoactivation was performed at apical side or basal side of cells, as described above. Immediately, the single-slice images of apical or basal cell edges were acquired in the mCherry channel and laser ablations were performed at the sixth frame with ∼60-70 mW of average laser power (50%) at 800 nm at single cell edges using a multiphoton laser scanning microscope Zeiss LSM 710 NLO with a C-Apochromat 40×/1.2 W objective. The images were recorded every 0.2 s before and after ablation. Acquisition of the image frame, during which the cell edge was ablated, lasted 0.4 s. The two vertices of the ablated cell edges were manually tracked in the recorded images, and the vertex distance increase over time was measured using Fiji (Schindelin et al., 2012). The recoil velocity was obtained by measuring the vertex distance increase at the first frame after ablation divided by 0.4 s. The recoil velocity is taken as a measure of relative mechanical tension on the cell edge before ablation (Ma et al., 2009). In the control experiment, no photoactivation was performed prior to laser ablation.

Lateral

For lateral laser ablation experiments, wing discs were mounted in culture medium with their lateral sides facing to the objective as described previously (Sui et al., 2018). Cell lateral F-actin cables were visualized using MoeABD::mCherry. An initial *z*-stack in the mCherry channel (acquisition at 561 nm) was acquired (five slices, 1 µm spacing) before activation. A ROI was defined in the lateral side of wing discs excluding apical and basal surfaces. One activation cycle was performed across a 5 µm *z*-stack (five slices with 1 µm spacing) for 50 frames (total of 120 s) in the ROI at 950 nm with laser power set to 13 mW and scanning direction set to bidirectional, yielding a pixel dwell of 3.15 µs. Immediately after activation, the single slice images of lateral cell interfaces were acquired in the mCherry channel, and laser ablations at F-actin-accumulated lateral interfaces were performed in the sixth frame with ∼60-70 mW of average power (50%) at 800 nm using a multiphoton laser scanning microscope Zeiss LSM 710 NLO with a C-Apochromat 40×/1.2 W objective. The images were recorded every 2 s at each frame. The apical and basal vertices of ablated lateral cell edges were manually tracked in the recorded images and the vertex distance increase over time was measured using Fiji. The recoil velocity was obtained by measuring the vertex distance increase at the first frame after ablation divided by 2 s. No photoactivation was performed prior to laser ablation in the control experiment.

Measurements of MoeABD::mCherry intensity

To quantify the ratio of MoeABD::mCherry pixel intensity in activated and non-activated regions over time upon apical or basal photoactivation, wing discs were mounted with their apical or basal side facing the objective, respectively. A *z*-stack of five apical or basal slices was obtained in the mCherry channel before activation. Then, one cycle of apical or basal photoactivation was performed in the ROI as described above. Subsequently, *z*-stacks, as described above, were acquired at 30 s intervals. The apical or basal MoeABD::mCherry maximum pixel intensity was obtained by projecting three to five slices of apical or basal *z*-stacks using the projection tool in Fiji (Schindelin et al., 2012). A rectangular ROI was defined in the activated region and in a neighboring non-activated region. The average MoeABD::mCherry pixel intensity was measured at the two regions over time using the plot function of Fiji (Schindelin et al., 2012), and the ratio of MoeABD::mCherry intensities in the activated and non-activated region was calculated.

To quantify the ratio of MoeABD::mCherry pixel intensity in activated and non-activated regions over time upon lateral photoactivation, wing discs were mounted with their apical side facing the objective. An image *z*-stack

Development (2020) 147, dev194316. doi:10.1242/dev.194316

from the apical to the basal surface of the cells was obtained in the mCherry channel before photoactivation. Then, one cycle of lateral photoactivation was performed in the ROI, as described above. Subsequently, whole cell *z*-stacks in the mCherry channel were obtained again at 30 s intervals after activation. MoeABD::mCherry pixel intensity was measured from cross-sections of wing discs. Rectangular ROIs were defined in the activated region and in a non-activated region in the cross-sections of wing discs. The average MoeABD::mCherry pixel intensity was measured at the two regions over time using the plot function of Fiji (Schindelin et al., 2012), and the ratio of Moe-ABD::mCherry pixel intensities in the activated and non-activated region was calculated.

Measurements of apical or basal cross-sectional cell area

To measure the apical or basal cross-sectional cell area changes during apical or basal photoactivation, wing discs were mounted with their apical or basal side facing the objective, respectively. The apical or basal photoactivations were performed as described above. Image *z*-stacks comprising five apical or basal slices were captured in the CIBN::pmGFP channel every 4 s using a 950 nm wavelength laser during the 2 min of activation. The single apical or basal focal plane of activation was extracted from the *z*-stacks for each time frame, and the apical or basal areas of each cell within the activation region were measured by Fiji (Schindelin et al., 2012) over time.

Measurements of cell height

All cell height measurements were performed on cross-sectional images of wing discs. Apical and basal vertices of cells within the activated region were manually tracked over time according to the cell membrane marker Gap43::mCherry or the F-actin marker MoeABD::mCherry. The average apical-basal cross-section lengths of these cells were then calculated from the tracking. The apical and basal outlines of the tissue were identified manually. The apical and basal indentations of the wing discs were then extracted by calculating the distance between apical or basal vertices of cells within the center of the activated region and the apical or basal outline of the tissue, respectively.

De-noising images using content-aware image restoration

Owing to the sensitivity of the wing disc to light exposure and the limitation of scanning time, all time-lapse images were acquired with low laser power and a limited number of *z*-slices. To improve signal-to-noise and *z*-stack image quality, we decreased the noise of images using a recently introduced machine learning-based image restoration approach (content-aware image restoration, CARE; Weigert et al., 2018). The 3D training data for each of the markers used (MoeABD::mCherry, CIBN::pmGFP and Gap43::mCherry) was obtained as previously described (Sui et al., 2018). These corresponding networks were applied to rescaled *z*-stacks of raw time-lapse data, resulting in less noisy *z*-stack images with improved *z* axis resolution. The Python code for training CARE networks is available at http://csbdeep.bioimagecomputing.com/doc/.

Statistical analysis

The Mann–Whitney *U* test and the Wilcoxon signed-rank test were used for statistical analysis.

Acknowledgements

We thank Stefano De Renzis (EMBL), Elisabeth Knust (Max Planck Institute of Molecular Cell Biology and Genetics) and the Bloomington *Drosophila* Stock Center for fly stocks. We thank the light microscopy facilities of the Biotechnology Center at the TU Dresden and of the Max Planck Institute of Molecular Cell Biology and Genetics for technical assistance.

Competing interests

The authors declare no competing or financial interests.

Author contributions

Conceptualization: L.S., C.D.; Methodology: L.S., C.D.; Formal analysis: L.S., C.D.; Investigation: L.S.; Resources: C.D.; Writing - original draft: C.D.; Writing - review & editing: L.S., C.D.; Supervision: C.D.

Funding

This research received no specific grant from any funding agency in the public, commercial or not-for-profit sectors.

Supplementary information

Supplementary information available online at
https://dev.biologists.org/lookup/doi/10.1242/dev.194316.supplemental

Peer review history

The peer review history is available online at
https://dev.biologists.org/lookup/doi/10.1242/dev.194316.reviewer-comments.pdf

References

Agarwal, P. and Zaidel-Bar, R. (2019). Principles of actomyosin regulation *in vivo*. *Trends Cell Biol.* **29**, 150-163. doi:10.1016/j.tcb.2018.09.006

Ambrosini, A., Rayer, M., Monier, B. and Suzanne, M. (2019). Mechanical function of the nucleus in force generation during epithelial morphogenesis. *Dev. Cell* **50**, 197-211.e5. doi:10.1016/j.devcel.2019.05.027

Anlaş, A. A. and Nelson, C. M. (2018). Tissue mechanics regulates form, function, and dysfunction. *Curr. Opin. Cell Biol.* **54**, 98-105. doi:10.1016/j.ceb.2018.05.012

Booth, A. J. R., Blanchard, G. B., Adams, R. J. and Röper, K. (2014). A dynamic microtubule cytoskeleton directs medial actomyosin function during tube formation. *Dev. Cell* **29**, 562-576. doi:10.1016/j.devcel.2014.03.023

Brand, A. H. and Perrimon, N. (1993). Targeted gene expression as a means of altering cell fates and generating dominant phenotypes. *Development* **118**, 401-415.

Cavanaugh, K. E., Staddon, M. F., Munro, E., Banerjee, S. and Gardel, M. L. (2020). RhoA mediates epithelial cell shape changes via mechanosensitive endocytosis. *Dev. Cell* **52**, 152-166.e5. doi:/10.1016/j.devcel.2019.12.002

Chauhan, B., Plageman, T., Lou, M. and Lang, R. (2015). Chapter eleven - Epithelial morphogenesis: the mouse eye as a model system. *Curr. Top. Dev. Biol.* **111**, 375-399. doi:10.1016/bs.ctdb.2014.11.011

Cohen, S. M. (1993). Imaginal disc development. In *The Development of Drosophila Melanogaster* (ed. M. Bate and A. Martinez Arias), New York: Cold Spring Harbor Laboratory Press, pp. 747-841.

Eritano, A. S., Bromley, C. L., Bolea Albero, A., Schütz, L., Wen, F.-L., Takeda, M., Fukaya, T., Sami, M. M., Shibata, T., Lemke, S. et al. (2020). Tissue-scale mechanical coupling reduces morphogenetic noise to ensure precision during epithelial folding. *Dev. Cell* **53**, 212-228.e12. doi:10.1016/j.devcel.2020.02.012

Farhadifar, R., Röper, J.-C., Aigouy, B., Eaton, S. and Jülicher, F. (2007). The influence of cell mechanics, cell-cell interactions, and proliferation on epithelial packing. *Curr. Biol.* **17**, 2095-2104. doi:10.1016/j.cub.2007.11.049

Gilmour, D., Rembold, M. and Leptin, M. (2017). From morphogen to morphogenesis and back. *Nature* **541**, 311-320. doi:10.1038/nature21348

Gracia, M., Theis, S., Proag, A., Gay, G., Benassayag, C. and Suzanne, M. (2019). Mechanical impact of epithelial-mesenchymal transition on epithelial morphogenesis in *Drosophila*. *Nat. Commun.* **10**, 2951. doi:10.1038/s41467-019-10720-0

Guglielmi, G., Barry, J. D., Huber, W. and De Renzis, S. (2015). An optogenetic method to modulate cell contractility during tissue morphogenesis. *Dev. Cell* **35**, 646-660. doi:10.1016/j.devcel.2015.10.020

Heer, N. C. and Martin, A. C. (2017). Tension, contraction and tissue morphogenesis. *Development* **144**, 4249-4260. doi:10.1242/dev.151282

Izquierdo, E., Quinkler, T. and De Renzis, S. (2018). Guided morphogenesis through optogenetic activation of Rho signalling during early *Drosophila* embryogenesis. *Nat. Commun.* **9**, 2366. doi:10.1038/s41467-018-04754-z

Krueger, D., Izquierdo, E., Viswanathan, R., Hartmann, J., Pallares Cartes, C. and De Renzis, S. (2019). Principles and applications of optogenetics in developmental biology. *Development* **146**, dev175067. doi:10.1242/dev.175067

Long, K. R., Newland, B., Florio, M., Kalebic, N., Langen, B., Kolterer, A., Wimberger, P. and Huttner, W. B. (2018). Extracellular matrix components HAPLN1, Lumican, and collagen I cause hyaluronic acid-dependent folding of the developing human neocortex. *Neuron* **99**, 702-719.e6. doi:10.1016/j.neuron.2018.07.013

Ma, X., Lynch, H. E., Scully, P. C. and Hutson, M. S. (2009). Probing embryonic tissue mechanics with laser hole drilling. *Phys. Biol.* **6**, 036004. doi:10.1088/1478-3975/6/3/036004

Martin, A. C. and Goldstein, B. (2014). Apical constriction: themes and variations on a cellular mechanism driving morphogenesis. *Development* **141**, 1987-1998. doi:10.1242/dev.102228

Martin, A. C., Kaschube, M. and Wieschaus, E. F. (2009). Pulsed contractions of an actin-myosin network drive apical constriction. *Nature* **457**, 495-499. doi:10.1038/nature07522

McGuire, S. E., Le, P. T., Osborn, A. J., Matsumoto, K. and Davis, R. L. (2003). Spatiotemporal rescue of memory dysfunction in *Drosophila*. *Science* **302**, 1765-1768. doi:10.1126/science.1089035

Monier, B., Gettings, M., Gay, G., Mangeat, T., Schott, S., Guarner, A. and Suzanne, M. (2015). Apico-basal forces exerted by apoptotic cells drive epithelium folding. *Nature* **518**, 245-248. doi:10.1038/nature14152

Nikolopoulou, E., Galea, G. L., Rolo, A., Greene, N. D. E. and Copp, A. J. (2017). Neural tube closure: cellular, molecular and biomechanical mechanisms. *Development* **144**, 552-566. doi:10.1242/dev.145904

Pearl, E. J., Li, J. and Green, J. B. A. (2017). Cellular systems for epithelial invagination. *Philos. Trans. R. Soc. B Biol. Sci.* **372**, 20150526. doi:10.1098/rstb.2015.0526

Sawyer, J. M., Harrell, J. R., Shemer, G., Sullivan-Brown, J., Roh-Johnson, M. and Goldstein, B. (2010). Apical constriction: a cell shape change that can drive morphogenesis. *Dev. Biol.* **341**, 5-19. doi:10.1016/j.ydbio.2009.09.009

Schindelin, J., Arganda-Carreras, I., Frise, E., Kaynig, V., Longair, M., Pietzsch, T., Preibisch, S., Rueden, C., Saalfeld, S., Schmid, B. et al. (2012). Fiji: an open-source platform for biological-image analysis. *Nat. Methods* **9**, 676-682. doi:10.1038/nmeth.2019

Sherrard, K., Robin, F., Lemaire, P. and Munro, E. (2010). Sequential activation of apical and basolateral contractility drives ascidian endoderm invagination. *Curr. Biol.* **20**, 1499-1510. doi:10.1016/j.cub.2010.06.075

Shyer, A. E., Tallinen, T., Nerurkar, N. L., Wei, Z., Gil, E. S., Kaplan, D. L., Tabin, C. J. and Mahadevan, L. (2013). Villification: how the gut gets its villi. *Science* **342**, 212-218. doi:10.1126/science.1238842

Spencer, A. K., Siddiqui, B. A. and Thomas, J. H. (2015). Cell shape change and invagination of the cephalic furrow involves reorganization of F-actin. *Dev. Biol.* **402**, 192-207. doi:10.1016/j.ydbio.2015.03.022

Staddon, M. F., Cavanaugh, K. E., Munro, E. M., Gardel, M. L. and Banerjee, S. (2019). Mechanosensitive junction remodeling promotes robust epithelial morphogenesis. *Biophys. J.* **117**, 1739-1750. doi:10.1016/j.bpj.2019.09.027

Sui, L., Alt, S., Weigert, M., Dye, N., Eaton, S., Jug, F., Myers, E. W., Jülicher, F., Salbreux, G. and Dahmann, C. (2018). Differential lateral and basal tension drive folding of *Drosophila* wing discs through two distinct mechanisms. *Nat. Commun.* **9**, 4620. doi:10.1038/s41467-018-06497-3

Urbano, J. M., Naylor, H. W., Scarpa, E., Muresan, L. and Sanson, B. (2018). Suppression of epithelial folding at actomyosin-enriched compartment boundaries downstream of wingless signalling in *Drosophila*. *Development* **145**, dev155325. doi:10.1242/dev.155325

Wallingford, J. B., Niswander, L. A., Shaw, G. M. and Finnell, R. H. (2013). The continuing challenge of understanding, preventing, and treating neural tube defects. *Science* **339**, 1222002. doi:10.1126/science.1222002

Weigert, M., Schmidt, U., Boothe, T., Müller, A., Dibrov, A., Jain, A., Wilhelm, B., Schmidt, D., Broaddus, C., Culley, S. et al. (2018). Content-aware image restoration: pushing the limits of fluorescence microscopy. *Nat. Methods* **15**, 1090-1097. doi:10.1038/s41592-018-0216-7

Wen, F.-L., Wang, Y.-C. and Shibata, T. (2017). Epithelial folding driven by apical or basal-lateral modulation: geometric features, mechanical inference, and boundary effects. *Biophys. J.* **112**, 2683-2695. doi:10.1016/j.bpj.2017.05.012

Zartman, J. J. and Shvartsman, S. Y. (2010). Unit operations of tissue development: epithelial folding. *Annu. Rev. Chem. Biomol. Eng.* **1**, 231-246. doi:10.1146/annurev-chembioeng-073009-100919